| OF |

AD
A075388

END
DATE
FILMED
11-79
DDC
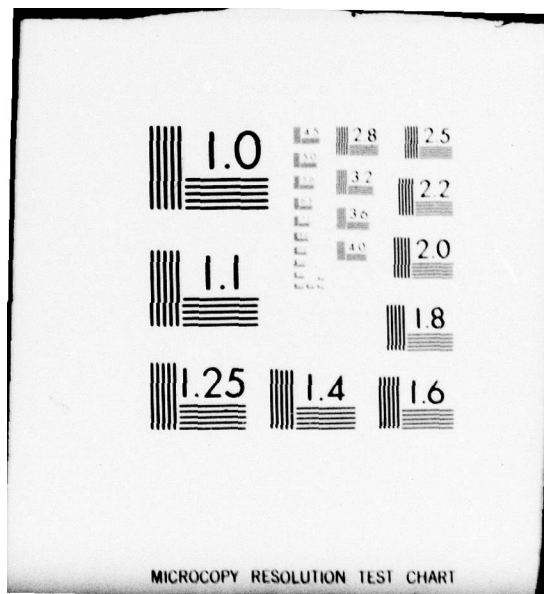
MICROCOPY RESOLUTION TEST CHART

LEVEL

EFFECT OF WORKPIECE PROPERTIES
ON GRINDING FORCES IN POLYCRYSTALLINE CERAMICS

Seventh Technical Report

By

B. G. Koepke and R. J. Stokes

Honeywell Corporate Materials Science Center

DDC
RECEIVED
OCT 23 1979
A

Honeywell Inc.
Corporate Materials Science Center
10701 Lyndale Ave. S.
Bloomington, Minnesota 55420

SECURITY CLASSIFICATION OF THIS PAGE (When Data Entered)

REPORT DOCUMENTATION PAGE		READ INSTRUCTIONS BEFORE COMPLETING FORM
1. REPORT NUMBER OP	2. GOVT ACCESSION NO.	3. RECIPIENT'S CATALOG NUMBER
4. TITLE (and Subtitle) Effect of Workpiece Properties on Grinding Forces in Polycrystalline Ceramics		5. TYPE OF REPORT & PERIOD COVERED
		6. PERFORMING ORG. REPORT NUMBER 47502 TR-7
7. AUTHOR(s) B.G. Koepke R.J. Stokes		8. CONTRACT OR GRANT NUMBER(s) Office of Naval Research Project N00014-69-C- 0123
9. PERFORMING ORGANIZATION NAME AND ADDRESS HONEYWELL Corporate Material Sciences Center 10701 Lyndale Av.S., Bloomington, MN 55420		10. PROGRAM ELEMENT, PROJECT, TASK AREA & WORK UNIT NUMBERS
11. CONTROLLING OFFICE NAME AND ADDRESS Office of Naval Research 800 North Qunicy Street Arlington, VA 22217		12. REPORT DATE June 1979
		13. NUMBER OF PAGES
14. MONITORING AGENCY NAME & ADDRESS(if different from Controlling Office) N00014-69-C-0123		15. SECURITY CLASS. (of this report) Unclassified
		15a. DECLASSIFICATION DOWNGRADING SCHEDULE

16. DISTRIBUTION STATEMENT (of this Report)

Report distributed according to list which is attached as last section, plus 30 copies internally within Honeywell.

17. DISTRIBUTION STATEMENT (of the abstract entered in Block 20, if different from Report)

Technical rept.,

18. SUPPLEMENTARY NOTES

19. KEY WORDS (Continue on reverse side if necessary and identify by block number)

Chip formation, grinding forces, surface condition, surface grinding

20. ABSTRACT (Continue on reverse side if necessary and identify by block number)

Grinding forces have been measured on a number of polycrystalline ceramics and correlations between the forces and workpiece properties have been attempted in an effort to gain insight into mechanisms of chip formation. The closest correlations were with a parameter related to the indentation fracture characteristics of each workpiece. This suggest that a major mechanism of chip formation during multipoint abrasive machining of ceramics is fracture

DD FORM 1473   EDITION OF 1 NOV 65 IS OBSOLETE
1 JAN 73

410 336

MIL-STD-847A
31 January 1973

20. Abstract
resulting from the plastic indentation of the workpiece by the abrasive grains. Grinding forces during up and down grinding were different but both correlated with the indentation fracture parameter when the comminution characteristics of the chips during down grinding were accounted for.

TABLE OF CONTENTS

LIST OF ILLUSTRATIONS

LIST OF TABLES

ABSTRACT

Grinding forces have been measured on a number of polycrystalline ceramics and corre-
lations between the forces and workpiece properties have been attempted in an effort to
gain insight into mechanisms of chip formation. The closest correlations were with a
parameter related to the indentation fracture characteristics of each workpiece. This
suggests that a major mechanism of chip formation during multipoint abrasive machining
of ceramics is fracture resulting from the plastic indentation of the workpiece by the
abrasive grains. Grinding forces during up and down grinding were different but both
correlated with the indentation fracture parameter when the comminution characteristics
of the chips during down grinding were accounted for.

1. INTRODUCTION

The quality and usefulness of a precision ceramic component may depend entirely on the abrasive machining operations used to shape and finish its surfaces. Yet it has been noted that abrasive surface finishing is still an "art based on experience" [1, 2][1]. There are good reasons for this comment. First, the mutual interactions between the components of a surface finishing system (eg - machine, tool, workpiece, environment, etc.) are complex and not well defined [2]. Second, the mechanisms whereby material is removed are not completely understood. For example finish surface grinding causes chip formation on an extremely fine scale at high rates under conditions of stress and temperature that are difficult to measure [2, 3].

Nevertheless considerable progress has been made since the first Symposium on the Science of Ceramic Machining and Surface Finishing [4]. It is now known that significant plastic flow may accompany chip formation during grinding of even the most brittle ceramics [5-8]. Scratch test studies [9, 10] and work using model grinding systems employing single point diamonds mounted on a grinding wheel [2, 11] have clearly shown that the mechanism of material removal depends on the normal force on the abrasive grain or, equivalently, on the depth of cut. At low loads material is removed by plastic flow, as the load increases cracking occurs and finally chips with dimensions larger than the abrasive grain form [10]. In a multipoint cutting process such as surface grinding, the subsurface interaction of the fractures due to chipping represent a major mechanism of material removal [10]. Single point grinding studies have further shown that chips can form in front of and behind the abrasive grain [3, 8], the latter presumably due to relaxation of stored elastic energy.

In view of the complexity of the situation the question arises as to whether there is any physical property or combination of physical properties which can be related to the forces involved in machining a particular ceramic. From the scratch test and single point grinding work it is recognized that the resistance to plastic flow and to fracture must both be included in any model of chip formation [2, 7-9]. Low speed scratch tests have shown that the forces vary with hardness when plastic flow is the dominant mode of material removal [9]. Gielisse et al. [11] have demonstrated in single point grinding that the forces vary as $\frac{\sigma^2}{2E}$ where σ is the fracture stress, and E Young's modulus when brittle fracture is the dominant mode of material removal.

---

[1]Figures in brackets indicate the literature references at the end of this paper.

1

Recent analyses of the relation of material properties and chip formation during ceramic machining have benefited from the indentation fracture theories of Lawn and coworkers [12, 13]. Evans and Wilshaw [13] have modelled abrasive machining as a series of sliding parallel indenters and have shown that the chip volume, V, is $V \sim P^{5/4} H^{-1/2} K_c^{-3/4}$ where P is the vertical load on the abrasive grain, H is the hardness and K_c is the fracture toughness. Sawing rate data of Fice and Speronello [14] fit this relation well. Kitchner et al. [15] have measured the depth of damage, c, introduced in Si_3N_4 during single point diamond grinding and have shown it to be related to the vertical grinding force, P, according to a relation derived by Lawn and Marshall [16] based on identation fracture theory $P \sim K_c c^{1/2}$. Thus, studies using single point abrasive systems and analyses incorporating the relatively new identation fracture theories have both led to an improved understanding of the important physical parameters determining material removal during abrasive machining of ceramics. Whether these results can be directly applied to multipoint machining operations such as surface grinding is questionable. The simultaneous interaction of adjacent abrasive grains during chip formation will alter the relative amounts of plastic flow and fracture and thus the resulting forces. Which fominates and under what conditions are not clear.

In this report we attempt to establish correlations by examining the effects of workpiece properties on forces generated during the surface grinding of a number of different ceramics. It was our hope that a clear correlation would establish the predominant mechanism of material removal under given conditions. Correlations are attempted between the forces and the workpiece properties to determine, at least, what properties most affect the mechanism of chip formation.

2. EXPERIMENTAL PROCEDURE

2.1 GRINDING

Grinding was carried out using a DoAll Model D618-7 high speed precision surface grinder with a fixed spindle speed of 3540 rpm. A 100 grit resinoid bond diamond wheel[2] 15.2 cm (6 inches) in diameter and 1.32 cm (1/8 inch) wide was used for all measurements. The cutting point density on the wheel face was 480 cm^{-2} and the mean width to depth ratio for a groove made by a single abrasive grain, as determined by techniques described by Backer, et al. [17] was 1.6. Grinding forces were measured with a strain gauge dynamometer based on a design of Cook et al. [18].   The dynamometer is similar to those used by others [2] and will not be discussed. With a sample mounted on the dynamometer, the horizontal and vertical grinding forces induced in the workpiece during a grinding pass can be measured independently. The elastic stiffness of the dynamometer is 1.2 x 10^5 gm/cm in the horizontal direction and 4.5 x 10^5 gm/cm in the vertical direction. The sensitivity of the instrument is 3 gm in both directions. Grinding was carried out both with the cutting face of the wheel moving in the same direction as the workpiece (down or climb grinding) and with the wheel moving in the opposite direction (up grinding). Different parts of the same workpiece were used for each case, i.e. one part of the surface was up ground and a separate part was down ground. Samples were ground at feed rates of 0.042, 0.21, and 0.42 cm/sec (1, 5 and 10 inches/min). The depth of cut was 25.4 μm (10^{-3} inches) except in one case where it was half this value. At least five passes were made at each feed rate and each sample was always ground at increasing rates of material removal. The wheel was dressed by grinding the face of the wheel with a silicon carbide wheel before each sample was ground at the lowest rate of material removal.

The theoretical chip geometry (i.e. chip length and maximum chip thickness) [17] for the grinding conditions used here are listed in Table 1.

Table 1. Theoretical maximum chip thickness, t, and chip length, ℓ, for the 100 grit diamond wheel at the machine settings used in this study.

Wheel	Depth of cut	Feed Rate (in/min)	t (μm)	ℓ (mm)
100 grit	25.4μm	0.042 cm/sec	0.32	2.0
		0.21	0.71	2.0
		0.42 cm/sec	1.0	2.0

[2]Do all type D1A1-MD100N/1DoB1/4B3

3

From Table 1 we note first that the grit depths of cut, t, are small and are on the order of 10^{-4} of the chip lengths. An indentation made by an abrasive grain on a ceramic workpiece is, therefore, no more than a long thin scratch [5, 9] provided material is removed by plastic flow. As noted above, however, if brittle fracture takes place during chip formation the actual chip geometry may in no way resemble the dimensions in Table 1 Note also that the small grit depth of cut indicates the advisability in many instances of using small wheel depths of cut. Otherwise a large amount of the binder in the wheel face may contact the workpiece.

Samples used for grinding were approximately 25.4 x 6.4 x 3.2 mm (1 x 1/4 x 1/8 inches). Grinding was carried out on the 25.4 x 6.4 mm side in the short (6.4mm) direction. All grinding was carried out dry.

2.2 CHARACTERIZATION OF THE GROUND SURFACE

Both optical and scanning electron microscopy were used for routine characterization of the surfaces produced by grinding. Most observations were made after the last pass at the highest feed rate of 0.42 cm/sec.

2.3 WORKPIECE MATERIALS

The materials machined in this study are listed in Table 2. Also included in the table are the supplier, method of manufacture and grain size.

4

Table 2. Materials used for Grinding Force Measurements

Material	Supplier	Manufacturing Method	Approximate Grain Size (μm)
PZT	Honeywell	Cold Pressed and Sintered	3
MgO	IITRI	Cold Pressed and Sintered	18
Ferrite NiZn	Honeywell	Hot Pressed	13
Ferrite NiZn	Honeywell	Hot Pressed	3
Silicon Nitride[a] "β"	Westinghouse	Hot Pressed	2
Silicon Nitride[a]	Norton	Hot Pressed	1
Silicon Nitride[a] "α"	Westinghouse	Hot Pressed	1
Lucalox Alumina	G.E.	Cold Pressed and Sintered	38
Alumina[b]	AVCO	Hot Pressed	2
AD 999 Alumina	Coors	Cold Pressed and Sintered	2
Boron Carbide[b]	AVCO	Hot Pressed	8

[a]Courtesy Dr. F. F. Lange
[b]Courtesy Dr. J. Niesse

The Westinghouse silicon nitrides listed in the table differ as follows [19, 20]. "β" Si_3N_4 was fabricated from powders containing 90% β-phase Si_3N_4 and 10% α-phase Si_3N_4. "α" Si_3N_4 was fabricated from powders containing 90% α-phase and 10% β-phase powder. All three materials were βphase after hot pressing. The three different Si_3N_4 materials are interesting because, as noted later, they exhibit measurably different properties.

5

3. EXPERIMENTAL RESULTS

3.1 GRINDING FORCE MEASUREMENTS

In order to conserve space the results are presented in tabular rather than graphical form although a few curves will be presented for illustrative purposes. The grinding force measurements are listed in the Appendix. Each value of force is normalized by the width of the cut, b, and is the average of five passes made at the depths of cut and feed rates indicated. Some brief comments concerning the force measurements are given below.

Grinding forces on PZT, MgO and the ferrites were extremely low and without exception increased with rate of material removal. The forces measured during up and down grinding were about equal. The vertical forces measured on the smaller grained ferrite exceeded those measured on the larger grained material. The horizontal forces measured on both ferrites were not a function of grain size.

The forces measured on Si_3N_4 during $25.4\mu m$ cuts were the highest measured in the series. In order to minimize damage to the dynamometer or wheel, measurements of the effect of rate of material removal on grinding forces were made using a cut of $12.2\mu m$. We note here that in a number of cases the vertical forces measured during down grinding exceeded those measured during up grinding in contrast to results on other hard ceramics such as B_4C and AVCO Al_2O_3. Examples of this behavior are shown in Figure 1 in which the grinding forces for the Westinghouse "α" Si_3N_4 are plotted as a function of feed rate during cuts of $12.2\mu m$.

The forces measured on alumina depended on fabrication. Sintered material such as Lucalox and Coors AD 999 showed low grinding forces at low feed rates but the forces increased rapidly with feed rate. AVCO hot pressed alumina on the other hand sustained a relatively high force level at all feed rates as indicated in Figure 2. The low sensitivity to feed rate during down grinding is not understood but may be related to the comminution characteristics of the chips as they travel between the wheel and the workpiece. This point is discussed later.

At the lowest feed rate the forces on B_4C during down grinding were greater than those during up grinding. This behavior reversed at the higher feed rates.

6

WESTINGHOUSE α PHASE Si_3N_4

○ DOWN
△ UP

Figure 1. Horizontal, $\frac{F_H}{b}$, and vertical, $\frac{F_v}{b}$, grinding forces
measured on Westinghouse "α" Si_3N_4 during up and down grinding
plotted as a function of workpiece feed rate. b is the width of the
cut. The depth of cut, d, is 12.2μm (0.005 inch).

AVCO Al$_2$O$_3$

o - DOWN
Δ - UP

GM / CM

F$_H$/b (GM/CM)

400

300

200

100

100 GRIT
d = 0.025mm

.1 .2 .3 .4 .5

V (cm/sec)

F$_V$/b (GM/CM)

1200

1000

800

600

400

200

100 GRIT
d = 0.025 mm

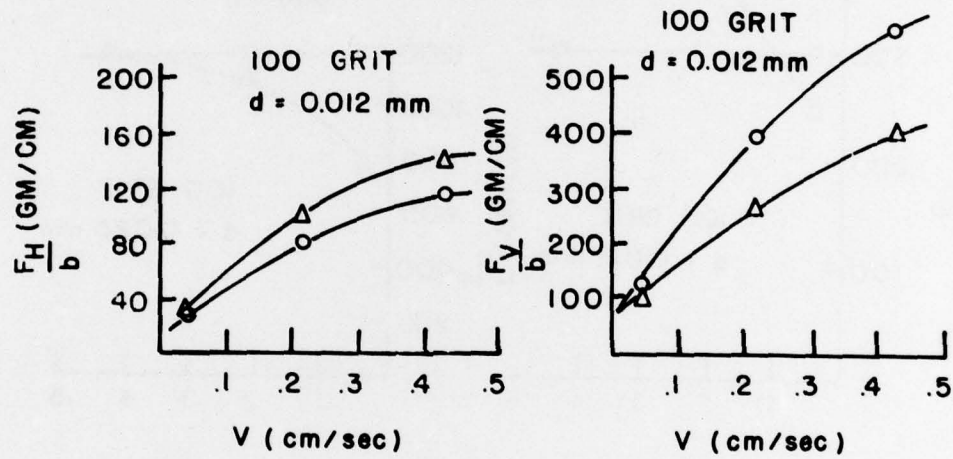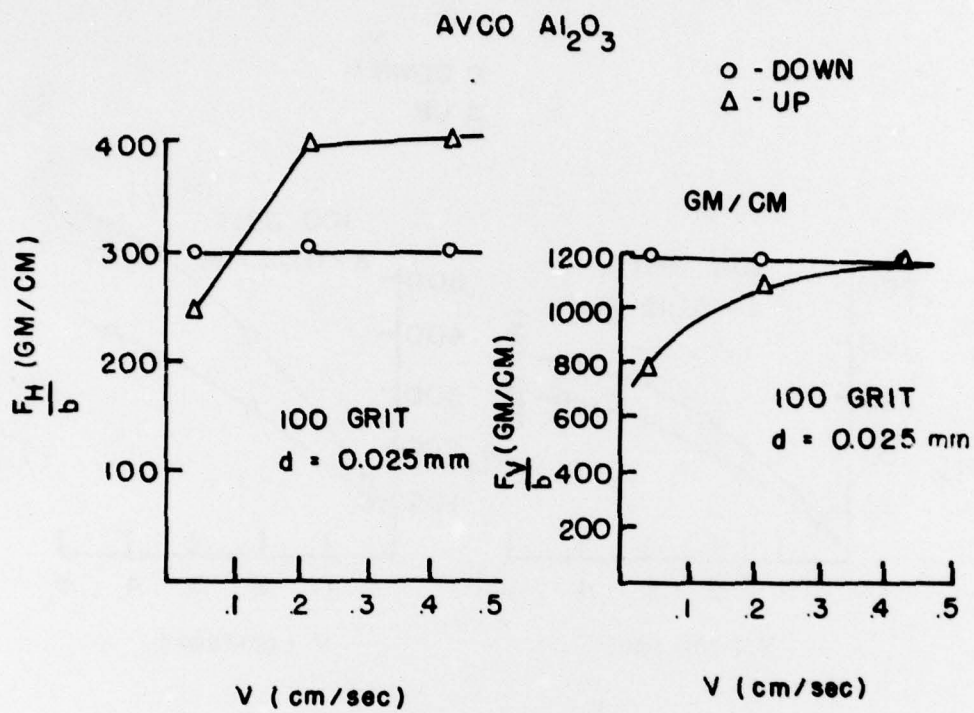.1 .2 .3 .4 .5

V (cm/sec)

Figure 2. Horizontal, $\frac{F_H}{b}$, and vertical, $\frac{F_v}{b}$, grinding forces measure on AVCO hot pressed Al$_2$O$_3$ during up and down grinding plotted as a function of workpiece feed rate. b is the width of the cut. The depth of cut, d, is 25.4μm (0.001 inch).

8

3.2 EXAMINATION OF THE GROUND SURFACES

The ground surfaces of every sample were examined following the last grinding force measurement which, as noted earlier, was made at the highest feed rate used in this work, 0.42 cm/sec. The nature of the surfaces will be commented on and illustrated in a few cases with scanning electron micrographs.

The ground surfaces of PZT were smooth and severely burnished. This accounts for the high grinding forces measured on this relatively soft ceramic.

The MgO surfaces were similar to the ferrite surfaces and contained plastically flowed regions and regions where material had been removed by brittle fracture. These surfaces are similar to those examined in an earlier study [6].

The large grained ferrite showed more intergranular fracture than plastically flowed material. The fine grained ferrite showed large flowed regions with some patches where material was removed by intergranular fracture. Examples of these surfaces are shown in Figure 3. Recall that the grinding forces on the fine grained material were slightly higher at the highest feed rate.

Without exception all silicon nitride surfaces were quite smooth and burnished and consisted mainly of plastically flowed regions. Patches where material was removed by what appeared to be intergranular fracture were seen scattered over every surface.

The sintered aluminas had surface features resembling the Si_3N_4 samples. A typical example is shown in Figure 4(a) for Coors AD 999 alumina down ground, 0.42 cm/sec. The irregular patches are where material has been removed by intergranular fracture. In contrast, the hot pressed alumina showed fewer burnished regions as shown in Figure 4(b). Most material has been removed by transgranular fracture. The B_4C surfaces were similar to those of Si_3N_4 and the sintered aluminas and contained regions of plastically flowed material and patches where material had been removed by brittle fracture. Due to a large amount of debris on the surfaces the nature of the fractures could not be assessed.

A few general comments concerning the nature of the ground surfaces are appropriate at this time. First, no significant differences were noted between surfaces produced by up and by down grinding. This was unexpected in view of the differences in forces observed. Second, all surfaces contained significant amounts of plastic flow. The large grained ferrite and hot pressed alumina contained less plastic flow than the others. Finally, it must be cautioned that the conditions observed here may not be identical to those obtained in actual practice. The samples were ground dry and were mounted on a dynamometer whose compliance is significantly greater than that of the machine table itself. Both dry grinding and a lower compliance may enhance burnishing.

9

GRINDING DIRECTION

20μm   20μm

(a)   (b)
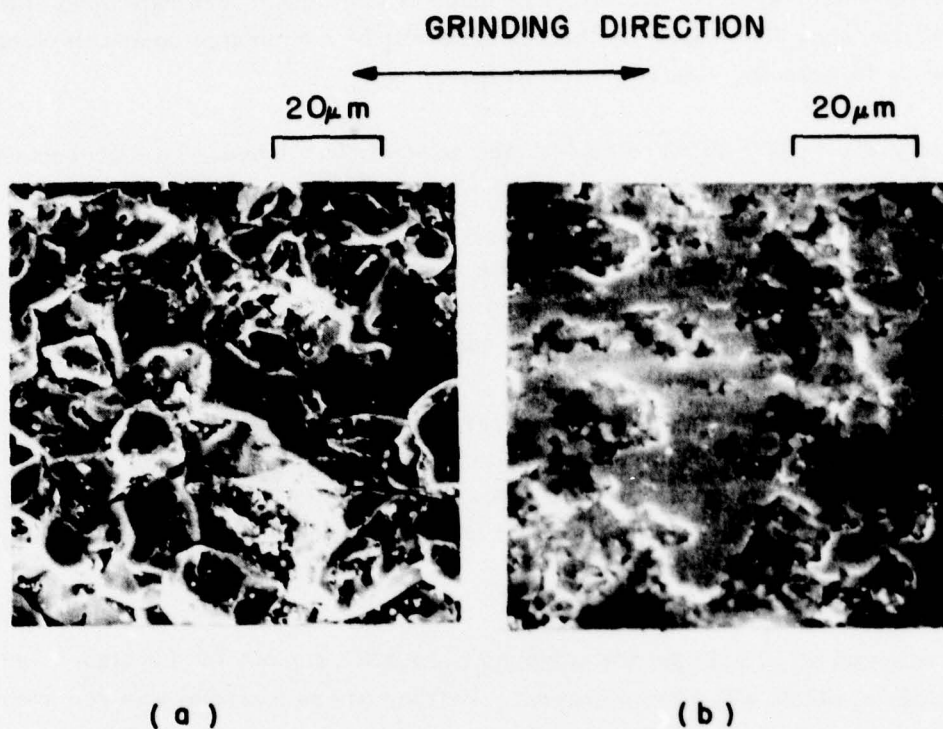
HOT PRESSED NiZnFERRITE

DOWN GROUND

$d = 25.4 \mu m$

$V = 0.42$ cm/sec

(a) 10μm G.S., (b) 3μm G.S.

Figure 3. Scanning electron micrographs of the ground surfaces of NiZn ferrite with mean grain sizes of (a) 10 and (b) 3μm

GRINDING DIRECTION

25μm   25μm

COORS AD999   AVCO HOT PRESSED
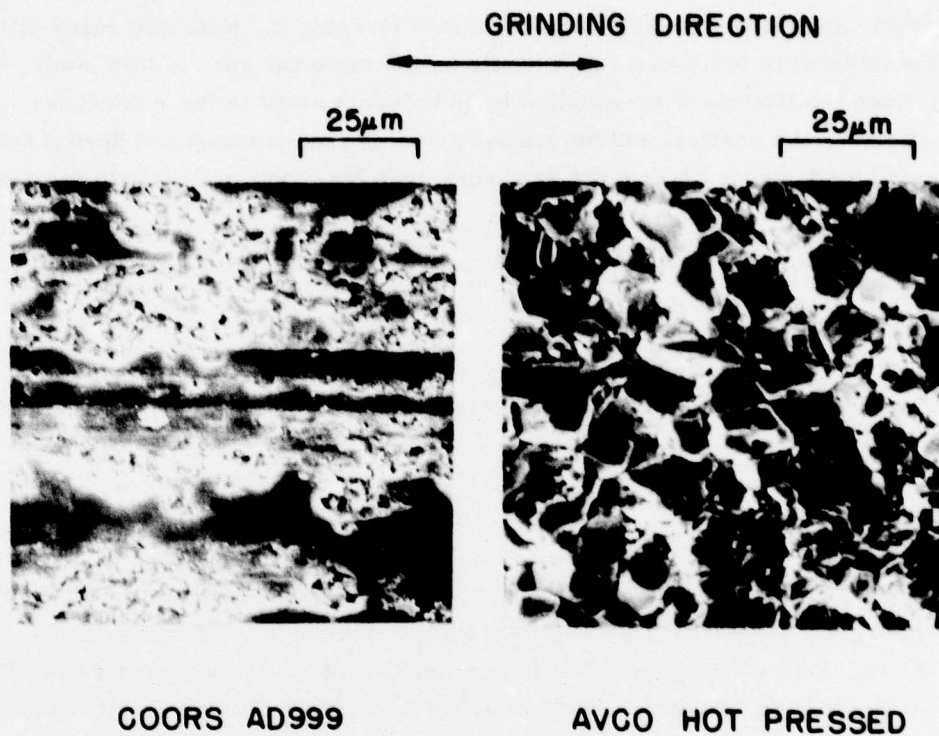
ALUMINUM OXIDE

DOWN GROUND

d = 25.4μm

V = 0.42 cm/sec

Figure 4. Scanning electron micrographs of the ground
surfaces of (a) Coors AD 999 alumina and (b) AVCO hot
pressed alumina.

11

4. GRINDING FORCE CORRELATIONS

The properties used for the correlations are listed in Table 3. Note that many of the
values in the table were not measured directly on the material used in this study, but
were taken from the literature or supplied by individuals noted in the references to the
table. In all cases the vertical and horizontal grinding forces measured during both up
and down grinding during a 25.4μm cut at a workpiece feed rate of 0.21 cm/sec were used
for correlations.

4.1 MELTING POINT

No obvious correlations with melting point were noted.

4.2 HARDNESS

Since hardness is an indication of resistance to plastic flow an examination of the relation
between grinding forces and hardness is warranted. The horizontal and vertical forces
measured during down grinding are shown as a function of workpiece hardness in Figure 5.
There is a trend toward increasing vertical grinding forces with hardness but the horizon-
tal forces drop in the harder materials. In both cases the highest grinding forces are
those measured on ceramics exhibiting intermediate values of hardness. Similar trends
were observed during up grinding but the forces measured on ceramics with intermediate
hardness were lower than those shown in Figure 5.

PZT
MgO
} FERRITE
Si_3N_4
Al_2O_3
B_4C

2000

1800

DOWN
GRINDING

1600

1400

1200

$\frac{F}{b}$ (GM/CM)

1000

800

$\frac{F_V}{b}$

600

400

$\frac{F_H}{b}$

200

KNOOP HARDNESS

1000   2000   3000

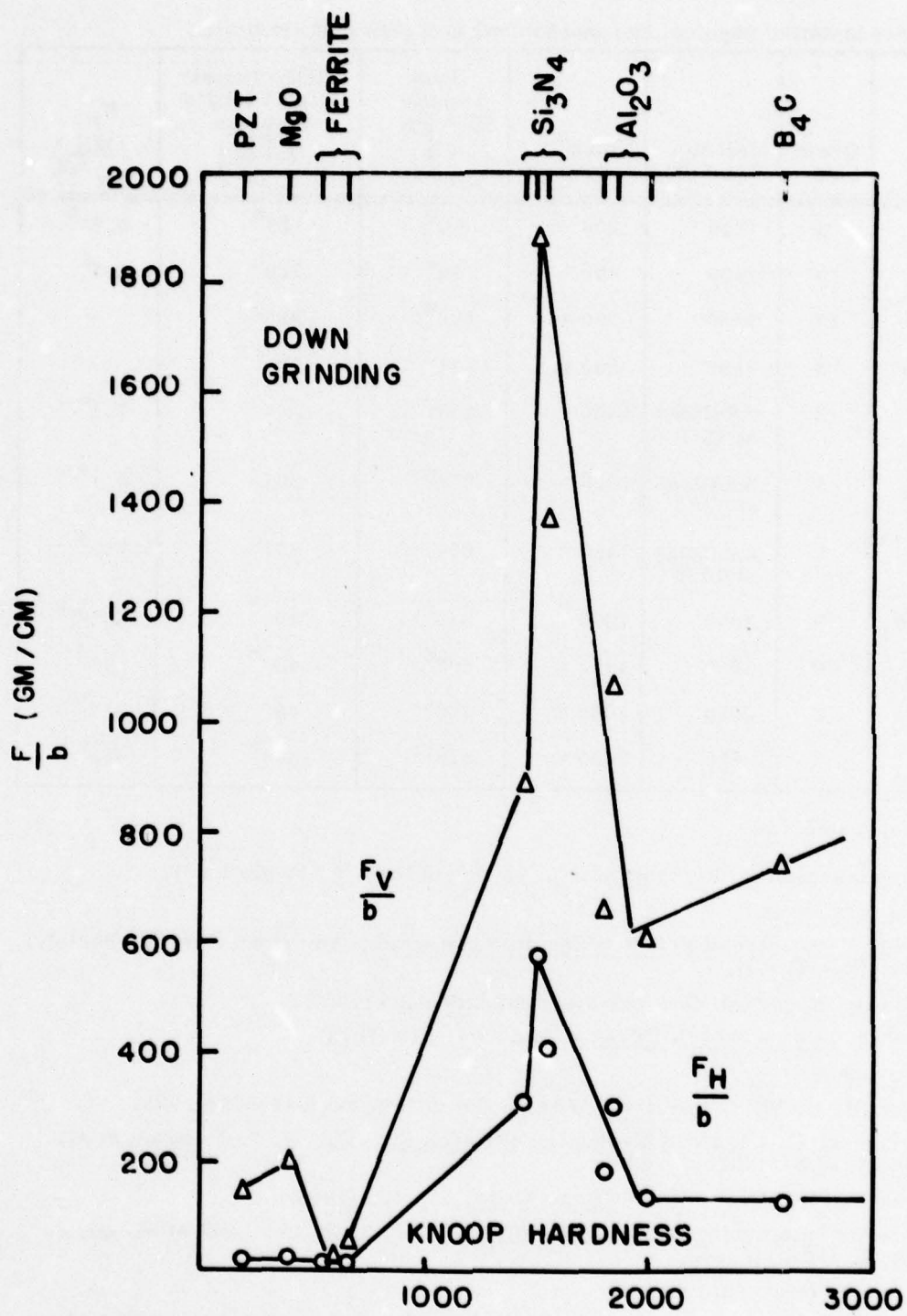Figure 5. Horizontal, $\frac{F_H}{b}$ and vertical, $\frac{F_V}{b}$, grinding forces measured during down grinding on different ceramics plotted as a function of workpiece hardness. The depth of cut and feedrate were 25.4μm and 0.21 cm/sec respectively.

13

Table 3. Representative physical and mechanical properties of ceramics.

Material	Grain Size	Melting Point ($^\circ$C)	Knoop[a] Hardness	Bend Tensile Strength $\left(\dfrac{MN}{m^2}\right)$	Polycrystalline Young's Modulus $\left(\dfrac{GN}{m^2}\right)$	K_{IC} $\left(\dfrac{MN}{m^{3/2}}\right)$
PZT	3	1300	200 *	55[b]	83[b]	0.75[h]
MgO	18	2850	400 *	28[c]	303[c]	2.5[i]
NiZn Ferrite	13	1660	550 #	166[d]	200[g]	-
NiZn Ferrite	3	1660	650 #	124[d]	200[g]	-
"β" Si_3N_4	2	Sublimes at 1870	1450 *	375[c]	307[e]	3.1[e]
Norton Si_3N_4	1	Sublimes at 1870	1500 *	676[c]	307[e]	5.1[e]
"α" Si_3N_4	1	Sublimes at 1870	1550 *	656[c]	307[e]	6.5[e]
Lucalox Al_2O_3	38	2050	1800 *	440[c]	400[c]	4.1[j,k]
AVCO Al_2O_3	10	2050	1850 *	407[f]	400[c]	6.5[l]
AD999 Al_2O_3	2	2050	2000 *	469[c]	400[c]	4.0[m]
B_4C	8	2350	2600 *	448[f]	448[c]	4.2[n]

References for Table 3.

a. All values measured in this laboratory. (# 100gm load, * 500 gm load).

b. Honeywell data sheet.

c. Engineering Properties of Selected Ceramic Materials, American Ceramic Society, Columbus, Ohio (1966).

d. M. Braitburg, Honeywell Inc. private communication (1972).

e. F. F. Lange, Journ. Amer. Ceram. Doc., 56, 518 (1973)

f. AVCO data sheet.

g. J. Smit and H. P. Wijn, Ferrites, Wiley & Sons, New York (1959) p. 225.

h. J. G. Bruce, et al. Fracture Mechanics of Ceramics, Vol. 4, R.C. Bradt et al. ed.. Plenum, N.Y. (1978) p. 696.

i. P. Gutshall and G. Gross, Eng. Fract. Mech., 1, 463 (1969).

j. R. F. Pabst, Fracture Mechanics of Ceramics, Vol. 2, R. C. Bradt et al. ed., Plenum N.Y. (1974) p. 557.

k. S. W. Freiman et al. ibid p. 666.

l. Measured in this laboratory by hardness identation technique of Evans and Charles, Journ. Amer. Ceram. Soc., 59, 371 (1976),

m. L. M. Barker, Fracture Mechanics of Ceramics, Vol. 4, R. C. Bradt, et al. ed., Plenum, N.Y. (1978) p. 490.

n. G. Gazza, Army Research Center, Watertown, MA., private communication (1972).

4.3 TENSILE STRENGTH

Grinding forces measured during down grinding are shown as a function of tensile strength in Figure 6. There is a trend for the forces to increase with strength but again the forces measured on materials with intermediate strengths are high. Similar behavior is observed when the forces measured during up grinding are plotted versus tensile strength.

4.4 POLYCRYSTALLINE YOUNG'S MODULUS

No correlations were noted but again the forces were highest on materials with interme-diate values of modulus, eg. Si_3N_4.

4.5 STRAIN ENERGY DENSITY, $\frac{\sigma^2}{2E}$

In single point diamond grinding studies on alumina workpieces Gielisse et al. [11] obtained excellent correlation between grinding forces and the strain energy density. $\frac{\sigma^2}{2E}$ where σ is the tensile strength and E is Young's modulus. No correlations were noted when the grinding forces measured in this work were plotted versus $\frac{\sigma^2}{2E}$.

4.6 FRACTURE TOUGHNESS

It can be argued that, if a major mechanism of material removal during grinding is the initiation and/or propagation of brittle cracks, then grinding forces should correlate with fracture toughness. Figure 7 shows that the grinding forces measured during up grinding do increase with the fracture toughness, but not linearly.

The grinding forces measured on Lucalox were low with respect to the other aluminas particularly during up grinding. The vertical forces measured on Lucalox are indicated on the plot. The low forces are attributed to the large grain size of this material.

Gielisse at al. [11] have noted a similar sharp decrease in forces during single point grinding of aluminas when the grain size exceeded about 20 μm.

No correlations between grinding forces measured during down grinding and K_{IC} were obtained.

15

2000

1800

1600 DOWN
GRINDING

1400

1200

$\frac{F}{b}$ (GM/CM)

1000

800

$\frac{F_V}{b}$

600

$\frac{F_H}{b}$

400

200

100 200 300 400 500 600 700

BEND TENSILE STRENGTH (MN, m^{-2})
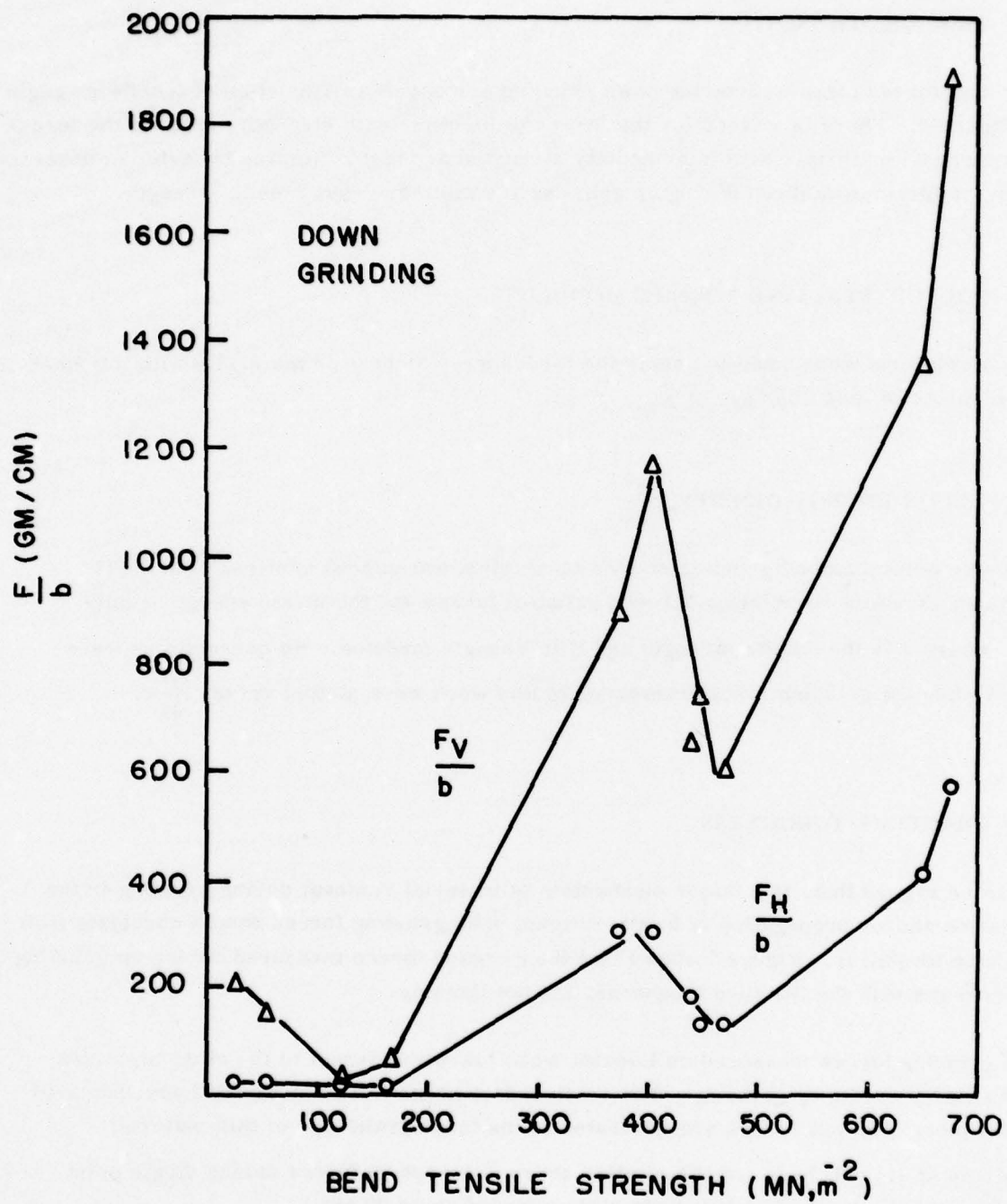
Figure 6. Horizontal and vertical grinding forces measured
on different ceramics plotted as a function of the bend tensile
strength of the workpiece materials. The depth of cut and
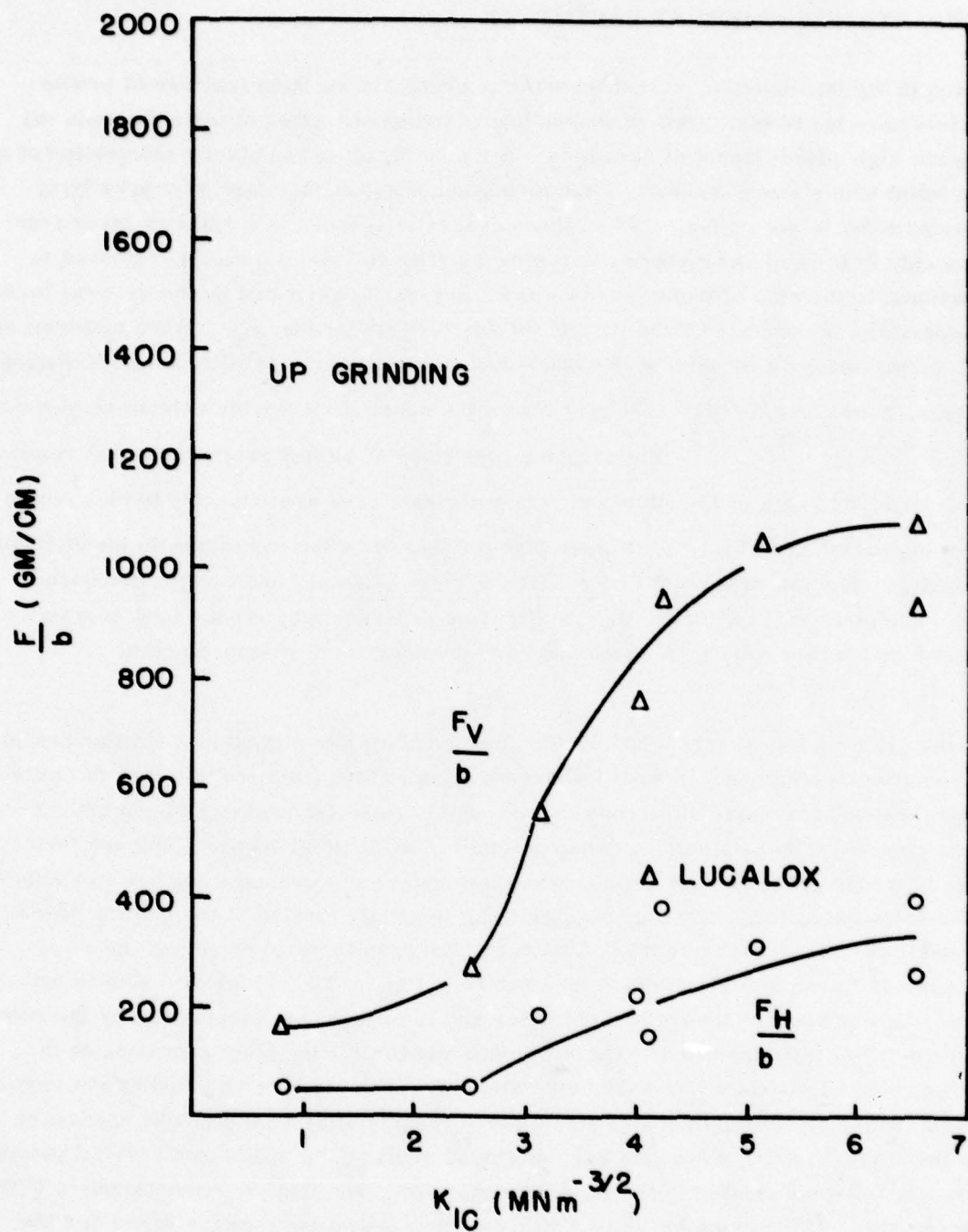feedrate were 25.4μm and 0.21 cm/sec respectively.

Figure 7. Horizontal and vertical grinding forces measured during up grinding on different ceramics plotted as a function of the fracture toughness, K_{IC}, of the workpiece materials. The depth of cut and feedrate were 25.4 μm and 0.21 cm/sec respectively.

17

4.7 INDENTATION FRACTURE PARAMETER

As noted in the Introduction, recent theories of plastic indentation fracture of brittle materials have led to increased understanding of the mechanisms of material removal during the high speed impact of ceramics. A major result of the plastic indentation of a brittle solid with a sharp indenter is the formation of subsurface lateral cracks lying roughly parallel to the surface. When these cracks intersect the surface or other fractures a chip is formed and material is removed. The volume of material removed is proportional to the size of these cracks which, in turn, is governed by the vertical force on the particle, P, the hardness, H, and the fracture toughness, K_C. When material removal during abrasive machining is assumed to take place by a parallel array of sliding indenters, Evans and Wilshaw [13] have shown the upper limit for the volume removed to be $V \sim P^{5/4} K_c^{-3/4} H^{-1/2}$. Thus, under conditions of a fixed rate of material removal, that is, fixed feed rate and depth of cut, the grinding forces are expected to be close to a linear function of $K_c^{3/4} H^{1/2}$. Figure 8 shows this to be the case for data taken during up grinding. The low data point represents the large grained Lucalox data discussed above. The high point is Norton Si_3N_4. Figure 8 represents by far the best correlation we have found between material properties and grinding force measurements.

When the grinding forces measured during down grinding are plotted in a similar fashion, no correlation is obtained. In what follows we attempt to rationalize this lack of correlation by considering a basic difference in the mode of material removal during up and down surface grinding of ceramics on a dynamometer. During up grinding, chips are formed at the leading edge of the contact area between the wheel and workpiece and are immediately ejected from the system. During down grinding the chips formed at the leading edge of the wheel-workpiece interface must first travel between the workpiece and the wheel to the back edge of the contact area before they can be ejected. The initial chip size in both cases is larger than the theoretical chip size and is presumably determined by the indentation fracture characteristics of the workpiece and the cutting point geometry on the wheel surface as discussed by Evans and Wilshaw. [13]. During up grinding the vertical grinding forces measured by the dynamometer depend mainly on the forces necessary to form the chips. During down grinding, on the other hand, the measured vertical grinding forces must also be related to the impact fracture or comminution characteristics of the isolated chips. If the chips break up readily as they travel between the wheel and the workpiece the vertical grinding forces will be reduced. If the chips do not break up readily high vertical grinding forces are expected. A parameter relating to the ability of a ceramic to resist impact fracture has been suggested by Clarke et. al. [21]. The number
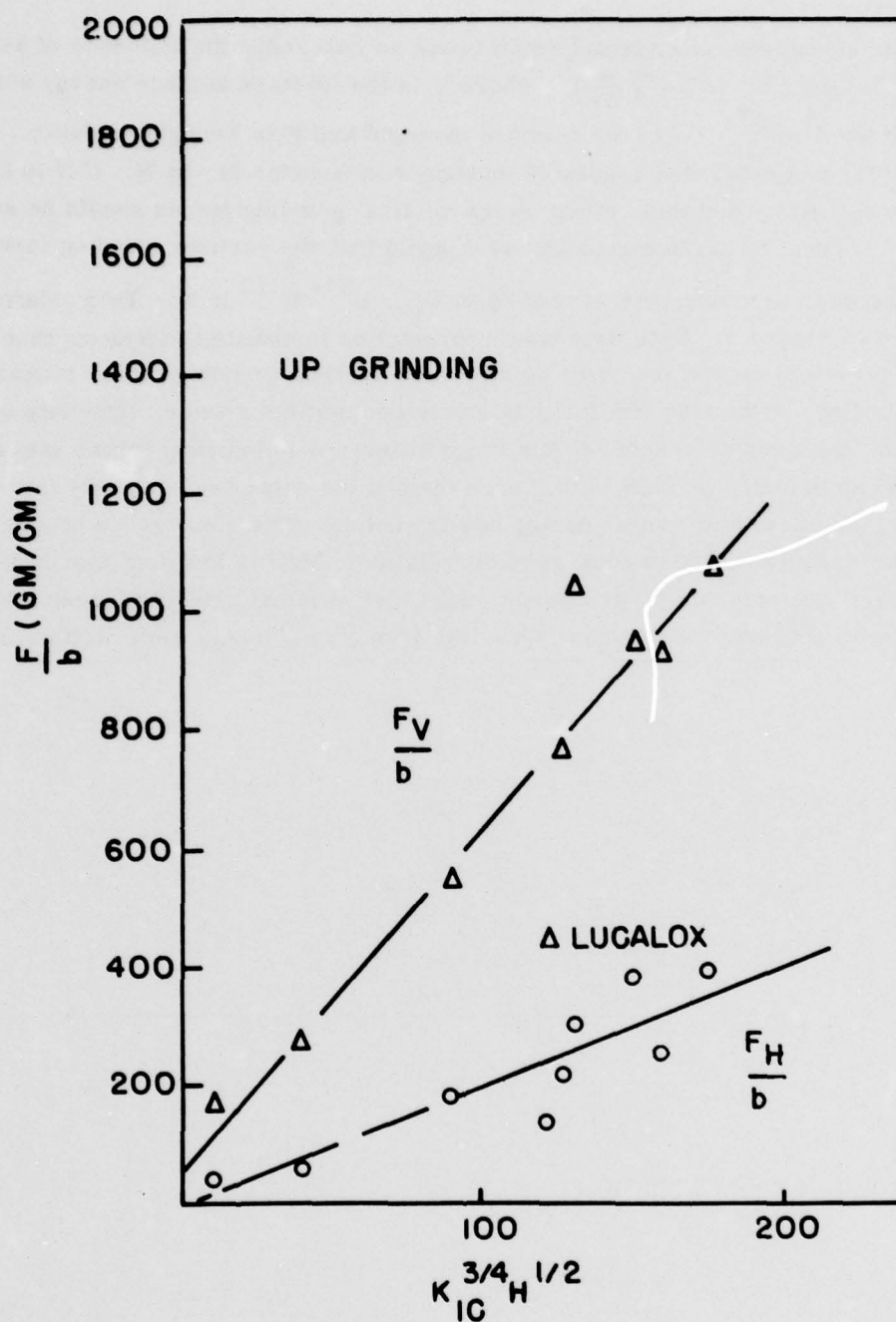
18

Figure 8. Horizontal and vertical grinding forces measured during up grinding on different ceramics plotted as a function of an indentation fracture parameter derived by Evans and Wilshaw [13]. K_{IC} is the fracture toughness and H is the Knoop hardness. The depth of cut and feedrate were 25.4μm and 0.21 cm/sec respectively.

19

of pieces a cubic centimeter of material would break up into under the influence of an elastic-energy density, W, is $N \sim \left(\frac{W}{6\gamma}\right)^3$ where γ is the fracture surface energy and W can be approximated by $\frac{\sigma^2}{2E}$. σ is the fracture strength and E is Young's modulus. Clarke et. al. [21] suggested that a suitable toughness parameter is $-\ln N$. If N is large the chips break up readily and their effect on the vertical grinding forces should be small. By relating this concept to surface grinding we suggest that the vertical grinding forces measured during down grinding vary according to $F_v \sim K^{3/4} H^{1/2} \ln N$. This relationship is shown plotted in Figure 9. Note first that a correlation is obtained indicating that the comminution characteristics of the chips do affect the vertical grinding forces measured during down grinding. Note also that the data are in two distinct groups. The data on Figure 9 suggest that a major reason for the large difference in grinding forces measured during down and up grinding on Si_3N is that once formed the chips break up only with much difficulty and cause high forces during down grinding. The other group of data including the aluminas and B_4C also show good correlation. MgO is low presumably because the chips are easily deformable [5] and do not cause high vertical grinding forces. No correlations were noted when the forces measured during up grinding were plotted in this manner.
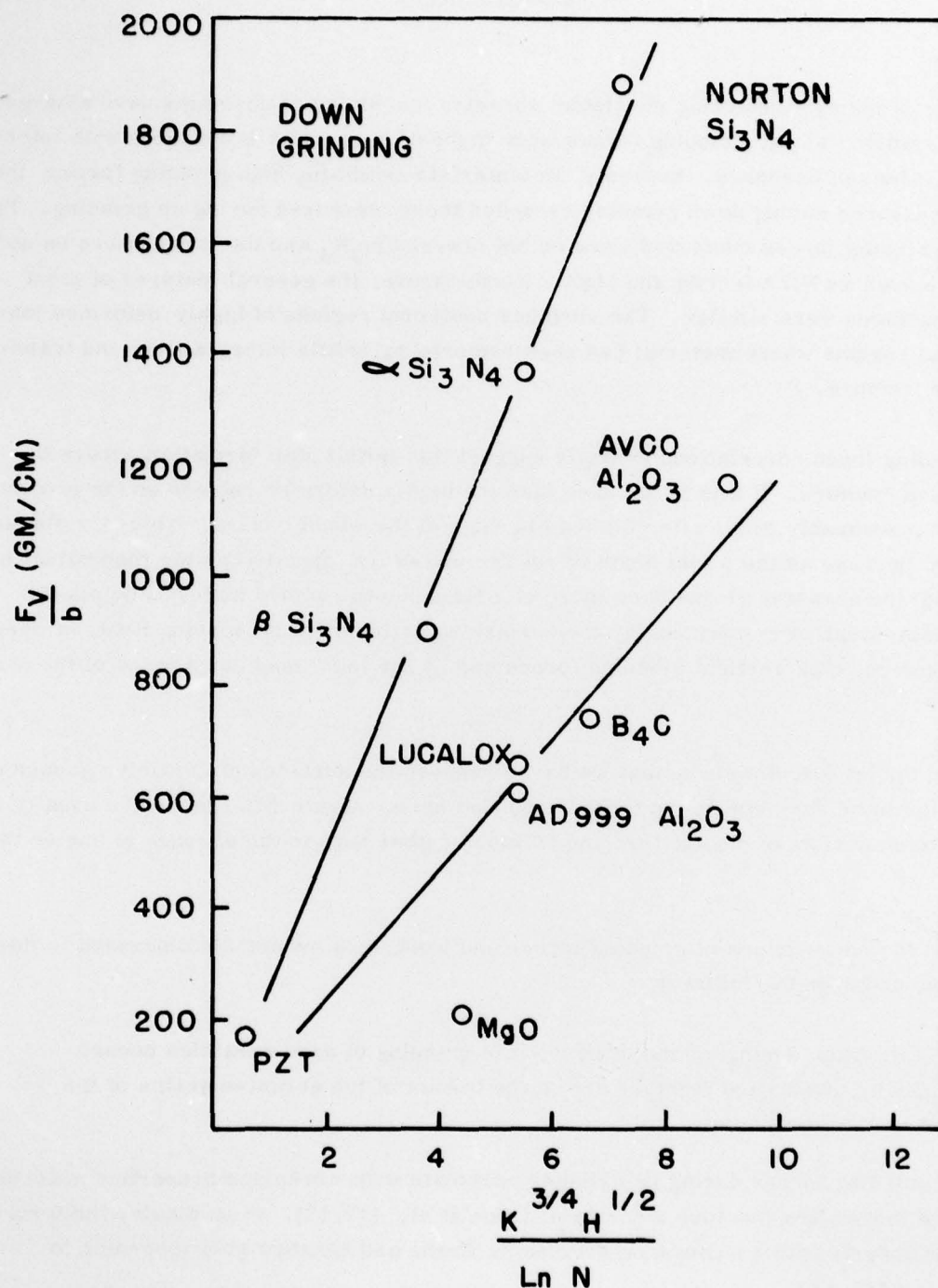
Figure 9. Vertical grinding forces measured during down grinding on different ceramics plotted as a function of the indentation fracture parameter of Evans and Wilshaw [13] divided by a toughness parameter suggested by Clarke et al. [21] that can be related to the comminution characteristics of the chips.

21

5. CONCLUSIONS

A number of points concerning multipoint abrasive machining of ceramics have emerged from this work. First, grinding forces were highest on ceramic workpieces with intermediate values of hardness. Secondly, in materials exhibiting high grinding forces, the forces measured during down grinding exceeded those measured during up grinding. The highest grinding forces measured were on hot pressed Si_3N_4 and the lowest were on softer ceramics such as NiZn ferrite and MgO. Furthermore, the general features of most ground surfaces were similar. The surfaces contained regions of highly deformed material and regions where material had been removed by brittle intergranular and transgranular fracture.

The grinding force correlations strongly suggest that initial chip formation occurs by indentation fracture. If this is the case then the highly deformed regions on the ground surfaces presumably occur after the leading edge of the wheel passes. This is a plausible argument because as the wheel depth of cut decreases (ie. approaches the theoretical chip thickness) the abrasive grains have more of a tendency to remove material by plastic flow. This situation is enhanced by the burnishing action of swarf moving between wheel and workpiece, high vertical grinding forces and by the increased compliance of the dynamometer.

We should point out, however, that we have observed the surfaces of ceramics ground on stiff tables to be very similar to those discussed here. Major differences are usually in the relative amounts of plastic flow and fracture rather than in the absence of one or the other.

Based on the correlations of grinding forces and workpiece properties discussed in this report we conclude the following:

1. Chip formation during up and down surface grinding of hard ceramics occurs initially by indentation fracture due to the impact of the abrasive grains of the wheel on the workpiece.

2. The grinding forces during up grinding correlate with workpiece properties according to the indentation fracture theories of Lawn et al. [12, 13]. In particular the forces vary linearly with a parameter derived by Evans and Wilshaw [13] according to $F \sim K_c^{3/4} H^{1/2}$ where K_c is the fracture toughness and H is the hardness.

3. Grinding forces during down grinding differ from those during up grinding because the chips formed at the leading edge of the wheel-workpiece interface must travel between the wheel and workpiece before being ejected from the system. This results in an increased vertical force that can be accounted for in different ceramics by considering the comminution characteristics of each material.

22

4. In every case the ground surfaces contained regions that were plastically flowed and regions where material had been removed by brittle fracture. It is suggested that a large amount of deformation occurred after the leading edge of the wheel had passed.

5. Because of the complexity of the cutting point geometry on a grinding wheel, grinding force measurements can only be used in a qualitative manner to examine mechanisms of material removal. Possibly a better and more direct approach is to measure the rates of material removal on different materials at constant force settings.

6. ACKNOWLEDGEMENTS

7. REFERENCES

1. Ceramic Processing, Publication 1576 (National Academy of Sciences, Washington, D.C., 1968) p. 145.

2. Gielisse, P.J. and Stanislao, J., Mechanical methods of surface finishing, in The Science of Ceramic Machining and Surface Finishing, S.J. Schneider and R.W. Rice, eds. pp. 5-35 (National Bureau of Standards, Washington, D.C., 1972).

3. Imanaka, O., Fugino, S. and Mineta, S., Direct observation of material removal process during grinding of ceramics by micro-flash technique, ibid pp. 37-43.

4. The Science of Ceramic Machining and Surface Finishing, S.J. Schneider and R.W. Rice, eds. (National Bureau of Standards, Washington, D.C. 1972).

5. Koepke, B.G. and Stokes, R.J., Grinding forces and the machining of magnesium oxide crystals, Journ. Mater. Sci., 7, [3], 485-493 (1972).

6. Koepke, B.G., An assessment of surface and subsurface damage introduced in ceramics by semifinish grinding operations, pp. 317-332 in Reference 4.

7. Hockey, B.J., Observations by transmission election microscopy on the subsurface damage produced in aluminum oxide by mechanical polishing and grinding, Proc. Brit. Ceram. Soc., 20, 95-115 (1972).

8. Becher, P.F., Ceramic machining and surface finishing, in Treatise on Materials Science and Technology, Vol. 9. Ceramic Fabrication Processes, F.F.Y. Wang ed., pp. 217-226. (Academic Press, New York, N.Y., 1976).

9. Broese van Groenou, A., Maan, N. and Veldkamp, J.D.B., Scratching experiments on various ceramic materials, Phillips Res. Rep., 30, [5], 320-359 (1975)

10. Broese van Groenou, A. and Veldkamp, J.D.B., Scratching and grinding parameters of various ferrites, Journ. Phys. (Paris), Colloq. [1] 285-289 (1977)

11. Gielisse, P.J., Kim, T.J. and Choudry, A., An experimental investigation of the dynamic and thermal characteristics of the ceramic stock removal process, in Materials Science and Research, Vol. 7. Surfaces and Interfaces of Glass and Ceramics, V.D. Frechette, W.C. LaCourse and V.L. Burdick eds. pp. 137-148 (Plenum Press, New York, N.Y. 1974)

12. Lawn, B. and Wilshaw, R., Indentation fracture: principles and applications, Journ. Mater. Sci., 10 [6], 1049-1081 (1975)

13. Evans, A.G., and Wilshaw, T.R., Quasi-static solid particle damage in brittle solids-I. observations, analysis and implications, <u>Acta Met.</u>, <u>24</u>, [10] 939-956 (1976)

14. Rice, R.W. and Speronello, B.K., <u>Journ. Amer. Ceram. Soc.</u>, <u>59</u>, [7-8], 330-333 (1976)

15. Kirchner, H.P., Gruver, R.M. and Richard, D., Fragment formation and damage penetration during abrasive machining of ceramics, Proc. 2nd Conf. on Science of Ceramic Machining and Surface Finishing, National Bureau of Standards, November (1978)

16. Lawn, B.R. and Marshall, D.B., Contact fracture resistance of physically and chemically tempered glass plates, a theoretical model, <u>Phys. Chem. Glasses</u>, <u>18</u>, [1], 7-18 (1977)

17. Backer, W.R., Marshall, E.R. and Shaw, M.C., The size effect in metal cutting. <u>Trans. Amer. Soc. Mech. Eng.</u>, <u>74</u> [1], 61-72 (1952)

18. Cook, N.H., Loewen, E.G. and Shaw, M.C., Machine - tool dynamometers: a current appraisal. <u>Amer. Mach.</u>, <u>98</u>, [10], 125-129 (1954)

19. Lange, F.F., Relation between strength, fracture energy and microstructure of hot-pressed Si_3N_4, <u>Journ. Amer. Ceram. Soc.</u>, <u>56</u>, [10], 518-522 (1973)

20. Lange, F.F., Strong, high-temperature ceramics, in <u>Annual Review of Materials Science, Vol. 4</u>, R.A. Huggins, R.H. Bube and R.W. Roberts, eds. pp. 365-390 (Annual Reviews Inc., Palo Alto, CA, 1974)

21. Clarke, F.J.P., Tattersall, H.G. and Tappin, G., Toughness of ceramics and their work of fracture, <u>Proc. Brit. Ceram. Soc.</u>, [6], 163-172 (1966)

26

8. APPENDIX

Horizontal, $\frac{F_H}{b}$, and vertical, $\frac{F_V}{b}$, grinding forces measured on a number of ceramics during down (wheel moving with workpiece travel) and up (wheel moving against workpiece travel) surface grinding with a 100 grit diamond wheel as a function of feed rate, b is the width of cut. The workpiece materials are listed in order of their hardness.

Material	Depth of Cut (mm)	Feed Rate (cm/sec)	Down Grinding		Up Grinding	
			$\frac{F_H}{b}$ (gm/cm)	$\frac{F_V}{b}$ (gm/cm)	$\frac{F_H}{b}$ (gm/cm)	$\frac{F_V}{b}$ (gm/cm)
PZT	.025	.042	12	74	17	72
		.21	25	153	40	165
		.42	42	220	59	236
MgO	.025	.042	6	79	11	93
		.21	24	208	51	265
		.42	44	268	74	312
NiZN Ferrite (13μm g.s.)	.025	.042	6	14	6	14
		.21	11	31	16	38
		.42	15	49	23	52
NiZN Ferrite (3μm g.s.)	.025	.042	8	27	9	30
		.21	14	66	20	74
		.42	16	88	27	101
"б" Si_3N_4	.025	.21	306	895	183	551
	.012	.042	31	106	34	106
		.21	87	311	84	271
		.42	128	429	125	399
Norton Si_3N_4	.025	.21	574	1883	312	1046
	.012	.042	56	361	100	370
		.21	84	493	126	505
		.42	113	562	153	659
'б" Si_3N_4	.025	.21	409	1362	254	934
	.012	.042	26	124	30	103
		.21	89	396	101	263
		.42	114	590	143	408

Material	Depth of Cut	Feed Rate	Down Grinding		Up Grinding	
Lucalox Al_2O_3	.025	.042	15	120	25	139
		.21	185	654	145	431
		.42	176	620	172	498
AVCO Al_2O_3	.025	.042	299	1184	249	775
		.21	303	1167	397	1071
		.42	293	1159	404	1156
Coors Al_2O_3	.025	.042	91	413	136	315
		.21	132	605	220	762
		.42	227	1005	311	1068
B_4C	.025	.042	73	523	43	154
		.21	129	740	386	942
		.42	152	838	415	1257

Technical and Summary Reports   June 1979

Organization	Copies	Organization	Copies
Defense Documentation Center Cameron Station Alexandria, VA 22314	12	Naval Air Propulsion Test Center Trenton, NJ 08628 ATTN: Library	1
Office of Naval Research Department of the Navy 800 N. Quincy Street Arlington, VA 22217		Naval Construction Batallion Civil Engineering Laboratory Port Hueneme, CA 93043 ATTN: Materials Division	1
ATTN: Code 471 Code 102 Code 470	1 1 1	Naval Electronics Laboratory San Diego, CA 92152 ATTN: Electron Materials Sciences Division	1
Commanding Officer Office of Naval Research Branch Office Building 114, Section D 666 Summer Street Boston, MA 02210	1	Naval Missile Center Materials Consultant Code 3312-1 Point Mugu, CA 92041	
Commanding Officer Office of Naval Research Branch Office 536 South Clark Street Chicago, IL 60605	1	Commanding Officer Naval Surface Weapons Center White Oak Laboratory Silver Spring, MD 20910 ATTN: Library	1
Office of Naval Research San Francisco Area Office One Hallidie Plaza Suite 601 San Francisco, CA 94102	1	David W. Taylor Naval Ship Research and Development Center Materials Department Annapolis, MD 21402	1
Naval Research Laboratory Washington, DC 20375		Naval Undersea Center San Diego, CA 92132 ATTN: Library	1
ATTN: Codes 6000 6100 6300 6400 2627	1 1 1 1 1	Naval Underwater System Center Newport, RI 02840 ATTN: Library	1
Naval Air Development Center Code 382 Warminster, PA 18964 ATTN: Mr. F. S. Williams	1	Naval Weapons Center China Lake, CA 93555 ATTN: Library	1
		Naval Postgraduate School Monterey, CA 93940 ATTN: Mechanical Engineering Department	1
Naval Air Systems Command Washington, DC 20360 ATTN: Codes 52031 52032	1	NASA Headquarters Washington DC 20546 ATTN: Code RRM	

BASIC DISTRIBUTION LIST (cont'd)

Organization	Copies	Organization	Copies
Naval Sea System Command Washington, DC 20362 ATTN: Code 035	1	NASA Lewis Research Center 21000 Brookpark Road Cleveland, OH 44135 ATTN: Library	1

Naval Facilities Engineering
  Command
Alexandria, VA 22331
ATTN: Code 03
	1	National Bureau of Standards
		Washington, DC 20234
		ATTN: Metallurgy Division
		        Inorganic Materials Div.
			1
			1

Scientific Advisor Commandant of the Marine Corps Washington, DC 20380 ATTN: Code AX	1	Director Applied Physics Laboratory University of Washington 1013 Northeast Fortieth Street Seattle, WA 98105	1
Naval Ship Engineering Center Department of the Navy Washington, DC 20360 ATTN: Code 6101	1	Defense Metals and Ceramics Information Center Battelle Memorial Institute 505 King Avenue Columbus, OH 43201	1
Army Research Office P.O. Box 12211 Triangle Park, NC 27709 ATTN: Metallurgy & Ceramics Program	1	Metals and Ceramics Division Oak Ridge National Laboratory P.O. Box X Oak Ridge, TN 37380	1
Army Materials and Mechanics Research Center Watertown, MA 02172 ATTN: Research Programs Office	1	Los Alamos Scientific Laboratory P.O. Box 1663 Los Alamos, NM 87544 ATTN: Report Librarian	1

Air Force Office of Schientific
  Research
Bldg. 410
Bolling Air Force Base
Washington, DC 20332
ATTN: Chemical Science Directorate
        Electronics & Solid State
          Sciences Directorate
	1
	
	1
		Argonne National Laboratory
		Metallurgy Division
		P.O. Box 229
		Lemont, IL 60439
			1

Air Force Materials Laboratory Wright-Patterson AFB Dayton, OH 45433	1	Brookhaven National Laboratory Technical Information Division Upton, Long Island New York 11973 ATTN: Research Library	1
Library Building 50, Rm 134 Lawrence Radiation Laboratory Berkeley, CA	1	Office of Naval Research Branch Office 1030 East Green Street Pasadena, CA 91106	1

Technical and Summary Reports

Organization	No. of Copies	Organization	No. of Copies
Dr. W.F. Adler Effects Technology Inc. 5383 Hollister Avenue P.O. Box 30400 Santa Barbara, CA 92105	1	Professor A.H. Heuer Case Western Reserve University University Circle Cleveland, OH 44106	1
Dr. G. Bansal Battelle 505 King Avenue Columbus, OH 43201	1	Dr. R. Hoagland Battelle 505 King Avenue Columbus, OH 43201	1
Dr. R. Bratton Westinghouse Research Lab. Pittsburgh, PA 15235	1	Dr. R. Jaffee Electric Power Research Institute Palo Alto, CA	1
Dr. A.G. Evans Rockwell International P.O. Box 1085 1049 Camino Dos Rios Thousand Oaks, CA 91360	1	Dr. P. Jorgensen Stanford Research Institute Poulter Laboratory Menlo Park, CA 94025	1
Mr. E. Fisher Ford Motor Co. Dearborn, MI	1	Dr. R.N. Katz Army Materials and Mechanics Research Center Watertown, MA 02171	1
Dr. P. Gielisse University of Rhode Island Kingston, RI 02881	1	Dr. H. Kirchner Ceramic Finishing Company P.O. Box 498 State College, PA 16801	1
Dr. M.E. Gulden International Harvester Company Solar Division 2200 Pacific Highway San Diego, CA 92138	1	Dr. B. Koepke Honeywell, Inc. Corporate Research Center 500 Washington Avenue South Hopkins, MN 55343	1
Dr. D.P.H. Hasselman Montana Energy and MHD Research and Development Institute P.O. Box 3809 Butte, Montana 59701	1	Mr. Frank Koubek Naval Surface Weapons Center White Oak Laboratory Silver Spring, MD 20910	1
Mr. G. Hayes Naval Weapons Center China Lake, CA 93555	1	E. Krafft Carborundum Co. Niagara Falls, NY	1
Dr. F.F. Lange Rockwell International P.O. Box 1085 1049 Camino Dos Rios Thousand Oaks, CA 91360	1	Dr. J. Ritter University of Massachusetts Department of Mechanical Engineering Amherst, MA 01002	1
Dr. J. Lankford Southwest Research Institute 8500 Culebra Road San Antonio, TX 78284	1	Professor R. Roy Pennsylvania State University Materials Research Laboratory University Park, PA 16802	1

Organization	No. of Copies	Organization	No. of Copies
Library Norton Company Industrial Ceramics Division Worcester, MA 01606	1	Dr. R. Ruh AFML Wright-Patterson AFB Dayton, OH 45433	1
State University of New York College of Ceramics at Alfred University Attn: Library Alfred, NY 14802	1	Mr. J. Schuldies AiResearch Phoenix, AZ	1
Dr. L. Hench University of Florida Ceramics Division Gainesville, FL 32601	1	Professor G. Sines University of California, Los Angeles Los Angeles, CA 90024	1
Dr. N. MacMillan Materials Research Laboratory Pennsylvania State University College Park, PA 16802	1	Dr. N. Tallan AFML Wright-Patterson AFB Dayton, OH 45433	1
Mr. F. Markarian Naval Weapons Center China Lake, CA 93555	1	Dr. T. Vasilos AVCO Corporation Research and Advanced Development Division 201 Lowell Street Wilmington, MA 01887	1
Dr. Perry A. Miles Raytheon Company Research Division 28 Seyon Street Waltham, MA 02154	1	Mr. J.D. Walton Engineering Experiment Station George Institute of Technology Atlanta, GA 30332	1
Mr. R. Rice Naval Research Laboratory Code 6360 Washington, DC 20375	1	Dr. S.M. Widerhorn Inorganic Materials Division National Bureau of Standards Washington, DC 20234	1
Dr. S.A. Bortz IITRI 10 W. 35th Street Chicago, IL 60616	1	Major W. Simmons Air Force Office of Scientific Research Building 410 Bolling Air Force Base Washington, DC 20332	1
Mr. G. Schmitt Air Force Materials Laboratory Wright-Patterson AFB Dayton, OH 45433	1	Dr. P. Becher Naval Research Laboratory Code 6362 Washington, DC 20375	
Dr. D.A. Shockey Stanford Research Institute Poulter Laboratory Menlo Park, CA 94025	1	Mr. L.B. Weckesser Applied Physics Laboratory Johns Hopkins Road Laurel, MD 20810	1
Dr. W.G.D. Frederick Air Force Materials Laboratory Wright-Patterson AFB Dayton, OH 45433	1	Mr. D. Richarson AiResearch Manufacturing Company 4023 36th Street P.O. Box 5217 Phoenix, AZ 85010	1

Organization	No. of Copies	Organization	No. of Copies
Dr. P. Land Air Force Materials Laboratory Wright-Patterson AFB Dayton, OH 45433	1	Dr. H.E. Bennett Naval Weapons Center Code 3818 China Lake, CA 93555	1
Mr. K. Letson Redstone Arsenal Huntsville, AL 35809	1	Mr. G. Denman Air Force Materials Laboratory Code LPJ Wright-Patterson AFB Dayton, OH 45433	1
Dr. S. Freiman Naval Research Laboratory Code 6363 Washington, DC 20375	1	Dr. D. Godfrey Admiralty Materials Laboratory Polle, Dorset BH16 6JU UNITED KINGDOM	1
Director Materials Sciences Defense Advanced Research Projects Agency 1400 Wilson Boulevard Arlington, VA 22209	1	Dr. N. Corney Ministry of Defense The Adelphi John Adam Street London WC2N 6BB UNITED KINGDOM	1
Dr. James Pappis Raytheon Company Research Division 28 Seyon Street Waltham, MA 02154	1	Dr. George W. Taylor Princeton Resources, Inc. P.O. Box 211 Princeton, New Jersey 08540	1
Dr. L. M. Gillin Aeronautical Research Laboratory P.O. Box 4331 Fisherman's Bend Melbourne, VIC 3001 AUSTRALIA	1	Dr. Herb Moss RCA Laboratories Princeton, New Jersey 08540	1
Dr. G. Ewell MS6-D163 Hughes Aircraft Co. Centinela and Teale Streets Culver City, CA 90230	1		
Dr. R.E. Tressler Ceramic Science Section 226 Steidle Bldg. The Pennsylvania State Univ. University Park, PA 16802	1		
Dr. R.E. Newnham Materials Research Laboratory The Pennsylvania State University University Park, PA 11802	1		
Dr. K.D. McHenry Honeywell, Inc. Corporate Technology Center 10701 Lyndale Avenue South Bloomington, MN 55420	1		
Dr. R.A. Queeney Professor of Engineering Mechanics Hammond Bldg. The Pennsylvania State University University Park, PA 16802	1		

SUPPLEMENTARY DISTRIBUTION LIST

Technical and Summary Reports

Advanced Research Projects Agency
Materials Science Director
1400 Wilson Boulevard
Arlington, VA 22209

Professor Michael Bell
Yeshiva University
Belfer Graduate School of Science
Ne York, NY 10033

Dr. Don Berlincourt
Channel Products
16722 Park Circle Dr. W.
Chagrin Falls, OH 44022

Dr. J. V. Biggers
Pennsylvania State University
Materials Research Laboratory
University Park, PA 16802

Mr. George Boyer
Sensor Systems Program
Office of Naval Research
Code 222
Arlington, VA 22217

Professor R. Bradt
Ceramics Section
Materials Sciences Department
The Pennsylvania State University
University Park, PA 16802

Dr. Dean Buckner
Piezo Products Division
Gulton Industries
P.O. Box 4300
Fullerton, CA 92634

Dr. Robert Callahan
Channel Industries
839 Ward Drive
Box 3680
Santa Barbara, CA 93105

Professor L.E. Cross
The Pennsylvania State University
Materials Research Laboratory
University Park, PA 16802

Dr. J.H. Simmons
Ca tholic University of America
Washington, DC 20064

Dr. P.L. Smith
Naval Research Laboratory
Code 6361
Washington, DC 20375

Dr. Bernard Jaffe
232 Forbes Road
Bedford, OH 44146

Dr. R. Lapetina
Edo Western Corporation
2645 South 300 West
Salt Lake City, UT 84115

Mr. C. LeBlanc
Naval Underwater Systems Center
TD 121
Newport, RI 02840

Dr. R.E. Loehman
University of Florida
Ceramics Division
Gainsville, FL 32601

Professor P.B. Macedo
The Catholic University of America
Washington, DC 20017

Dr. N. Perrone
Code 474
Office of Naval Research
800 N. Quincy Street
Arlington, VA 22217

Dr. R. Pohanka
Naval Research Laboratory
Code 6130
Washington, DC 20375

Dr. Frank Recny
General Electric Company
Court Street
Plant Building C
Box 1122
Syracuse, NY 13201

Dr. J.H. Rosolowski
General Electric Company
Research and Development Center
P.O. Box 8
Schenectady, NY 02301

Mr. W.B. Crandall
Alfred University
Alfred, NY 14802

Dr. J.T.A. Roberts
Electric Power Research Institute
34-2 Hillview Ave.
P.O. Box 10412
Palo Alto, CA 94303

Technical and Summary Reports

Dr. R.W. Timme
Naval Research Laboratory
Code 8275
Underwater Sound Reference Division
P.O. Box 8337
Orlando, FL 32806

Dr. Charles C. Walker
Naval Sea Systems Command
National Center #3
2531 Jefferson Davis Highway
Arlington, VA 20390

Dr. Paul D. Wilcox
Sandia Laboratories
Division 2521
Albuquerque, NM 87115

Linda Husted
Librarian
Materials Sciences Corporation
Merion Towle Building
Blue Bell, PA 19422

Glove-Union, Inc.
5757 North Green Bay Avenue
Milwaukee, WI 53201
ATTN: G. Goodman

Dr. M. Noone
General Electric Company
Space Sciences Laboratory
Room M9539, P.O. Box 8555
Philadelphia, PA 19101

Dr. S.M. Wiederhorn
Inorganic Materials Division
National Bureau of Standards
Washington, D.C. 20234

Dr. C.O. Hulse
United Aircraft Research Labs
United Aircraft Corporation
East Hartford, CT 06108

Prof. M.H. Manghnani
University of Hawaii
Hawaii Institute of Geophysics
2525 Correa Road
Honolulu, HI 96822

Dr. Marvin Hass
Naval Research Laboratory
Code 6408
Washington, D.C. 20375

Dr. W.R. Manning
Champion Spark Plug Company
20000 Conner Ave.
Detroit, MI 48234

Dr. B.A. Wilcox
Ceramics Program, Room 336
Metallurgy and Materials Research
National Science Foundation
Washington, D.C. 20550

Dr. H.E. Bennett
Naval Surface Weapons Center
Research Department Code 601
China Lake, CA 93555

Dr. R.J. Charles
General Electric Company
Research and Development Center
Schenectady, NY 12301

Dr. A.R.C. Westwood
Martin-Marietta Laboratories
1450 South Rolling Road
Baltimore, MD 21227

Professor R.H. Doremus
Rensselaer Polytechnic Institute
Troy, NY 12181

Dr. D.E. Niesz
Battelle Memorial Institute
505 King Avenue
Columbus, OH 43201

Dr. S.M. Wiederhorn
Physical Properties Section
Bldg. 223, Rm. A355
National Bureau of Standards
Washington, D.C. 20234